Transcriptional Profiling after Lipid Raft Disruption in Keratinocytes Identifies Critical Mediators of Atopic Dermatitis Pathways

Conny Mathay[1], Michael Pierre[2], Mark R. Pittelkow[3], Eric Depiereux[2], Arjen F. Nikkels[4], Alain Colige[5] and Yves Poumay[1]

Lipid rafts are cholesterol-rich cell signaling platforms, and their physiological role can be explored by cholesterol depletion. To characterize transcriptional changes ongoing after lipid raft disruption in epidermal keratinocytes, a cell type that synthesizes its cholesterol *in situ*, we performed whole-genome expression profiling. Microarray results show that over 3,000 genes are differentially regulated. In particular, IL-8, urokinase-like plasminogen activator receptor, and metalloproteinases are highly upregulated after cholesterol extraction. Quantitative reverse transcriptase PCR validation and protein release measurements demonstrate the physiological relevance of microarray data. Major enriched terms and functions, determined by Ingenuity Pathways Analysis, identify cholesterol biosynthesis as a major function, illustrating the specificity of keratinocyte response toward cholesterol depletion. Moreover, the inflammatory skin disorder atopic dermatitis (AD) is identified as the disease most closely associated with the profile of lipid raft-disrupted keratinocytes. This finding is confirmed in skin of AD patients, in whom transcript levels of major lipid raft target genes are similarly regulated in lesional atopic skin, compared with non-lesional and normal skin. Thus, lipid raft disruption evokes typical features of AD, thereby suggesting that lipid raft organization and signaling could be perturbed in atopic keratinocytes.

Journal of Investigative Dermatology advance online publication, 30 September 2010; doi:10.1038/jid.2010.272

INTRODUCTION

As the existence of membrane lipid rafts is now established (Simons and Toomre, 2000; Foster, 2008), large-scale functional studies start unraveling the relevance of lipid rafts in cell signaling and physiology (Yaqoob and Shaikh, 2010). Presently, lipid rafts are defined as dynamic nanoscale membrane microdomains containing high amounts of cholesterol and sphingolipids that, on activation, coalesce into large signaling platforms (Pike, 2006, 2009). A regulated amount of cholesterol is crucial for all animal plasma membranes, as cholesterol helps in regulating the fluidity of the membrane. Moreover, the presence of membrane cholesterol and lipid raft existence is tightly related to cellular cholesterol biosynthesis (Lange *et al.*, 2004). In epidermis, cholesterol is also needed for the establishment of the cornified barrier (Wertz and Michniak, 2000), this tissue being an active site of cholesterol synthesis. Thus, numerous lipid raft aggregates have been found, for instance, in transit-amplifying keratinocytes (Gniadecki and Bang, 2003). Membrane cholesterol depletion by methyl-β-cyclodextrin (MBCD) is known to disrupt lipid rafts in keratinocytes (Kabouridis *et al.*, 2000; Jans *et al.*, 2004) and it has been shown that the signaling molecules p38 mitogen-activated protein kinase, extracellular signal-regulated kinase 1/2, and epidermal growth factor receptor (EGFR) are activated and that the expression of involucrin (IVL) and keratin 10, two epidermal differentiation markers, is altered after lipid raft disruption (Jans *et al.*, 2004; Lambert *et al.*, 2006; Mathay *et al.*, 2008). Parallelisms in response of keratinocytes to cholesterol depletion or to H_2O_2 suggested an involvement of oxidative mechanisms subsequent to lipid raft perturbation, but a panel of experimental data refuted that hypothesis (Mathay and Poumay, 2010). To acquire a global view of transcriptional changes occurring after lipid raft perturbation by cholesterol depletion, whole-genome transcriptional profiling in MBCD-treated keratinocytes was performed. This powerful technique combined with bioinformatics data analyses allows the identification and characterization of lipid raft-dependent transcriptional targets and cell signaling

[1]*Cell and Tissue Laboratory, URPHYM, University of Namur (FUNDP), Namur, Belgium;* [2]*Laboratory of Biostatistics and Bioinformatics, URBM, University of Namur (FUNDP), Namur, Belgium;* [3]*Departments of Dermatology and Biochemistry and Molecular Biology, Mayo Clinic, Rochester, Minnesota, USA;* [4]*Department of Dermatology, Centre Hospitalier Universitaire de Liège, University of Liège, Liège, Belgium and* [5]*Laboratory of Connective Tissues Biology, University of Liège, Liège, Belgium*

Correspondence: Yves Poumay, Cell and Tissue Laboratory, URPHYM, University of Namur (FUNDP), 61, Rue de Bruxelles, B-5000 Namur, Belgium. E-mail: yves.poumay@fundp.ac.be

Abbreviations: AD, atopic dermatitis; DRGs, differentially regulated genes; MBCD, methyl-β-cyclodextrin

Received 5 May 2010; revised 7 July 2010; accepted 28 July 2010

pathways, as well as association of functions and diseases with lipid raft-disrupted keratinocytes. Atopic dermatitis (AD), a skin disease characterized by allergic skin inflammation and dysfunctional epidermal barrier (Oyoshi *et al.*, 2009), shows strong parallelisms in expression profiles with lipid raft-disrupted keratinocytes. Skin biopsies of AD patients show that lipid raft disruption identifies critical mediators of certain AD pathways.

RESULTS

Transcriptional response of lipid raft-disrupted keratinocytes

The dynamics of keratinocyte response to lipid raft disruption by MBCD was evaluated by measuring transcript levels immediately after cholesterol depletion (R0h) or after recovery periods of 1 hour (R1h) and 8 hours (R8h). Time points were chosen in accordance with previous studies showing heparin-binding EGF-like growth factor (HB-EGF) gene regulation, together with alterations in epidermal differentiation markers IVL and keratin 10 (Mathay *et al.*, 2008). Analysis of transcripts encoded by these genes using microarray and real-time PCR and analysis of phosphorylation of EGFR, Akt, and p38 mitogen-activated protein kinase confirm the typical effects observed after cholesterol depletion (Supplementary Figure S1 online). Expression profiling in cholesterol-depleted keratinocytes shows that immediate–early gene response to MBCD is limited to 59 genes at R0h, 392 genes at R1h, but transcriptional changes representing 2,756 differentially regulated genes (DRGs) occur during the 8-hour recovery phase (Supplementary Figure S1 online). Conversely, mock cholesterol depletion by MBCD/cholesterol complexes induces a small number of DRGs only. Thus, for the clarity of data presentation, comparisons between MBCD versus control are solely illustrated. Complete lists of DRGs for keratinocytes treated with MBCD or cholesterol-loaded MBCD compared with controls are provided in Supplementary Figure S2 online.

Reflecting the biological relevance of gene regulation, DRGs were classified according to comparison fold changes as recommended by Shi *et al.* (2008). In Table 1, the 20 highest fold changes (up- and downregulation) for the comparison between MBCD versus control are shown for each recovery period. HB-EGF is identified among the major transcriptional targets at R0h and R1h after MBCD treatment. Similarly, IL genes are highly responsive toward membrane cholesterol depletion, with ILs *IL-8*, *IL-1B*, and *IL-20*, or Interleukin receptors *IL-13RA2*, *IL-1RL1*, and *IL-1R2*, being highly induced, especially at R8h. Most notably, proinflammatory cytokine *IL-8* is identified as the most highly induced gene at R1h, and is also highly induced at R8h. Other genes involved in the inflammatory response, including prostaglandin-endoperoxide synthase 2 (*PTGS2*; cyclooxygenase (*COX-2*)), plasminogen activator, urokinase receptor (*PLAUR*), and the metalloproteinases (*MMP1* and *MMP10*), are also highly induced. However potential inflammatory responses seem tightly regulated as the suppressor of cytokine signaling 3(*SOCS3*) and *IL-1RL1*, which functions as an anti-inflammatory receptor (Brint *et al.*, 2004), are also highly expressed after cholesterol depletion. Interestingly, members of the epidermal differentiation complex, filaggrin (*FLG*), *FLG-2* (a recently identified member of the epidermal differentiation complex; Wu *et al.*, 2009), and cornifelin, are strongly downregulated immediately after MBCD treatment. Furthermore, several zinc-finger transcription factors (*ZNF434*, *ZNF57*, *ZNF14*) are downregulated at R1h.

Real-time PCR validation of major MBCD-transcriptional targets

Transcript levels of several microarray-identified DRGs were investigated by quantitative real-time PCR to ensure the accuracy of genome expression profiling (Table 2). Gene selection was based on their biological importance in epidermal keratinocytes and on their differential expression in at least two analyzed time points. When comparing both techniques, expression values of all eight analyzed genes indicate regulations with same directions and levels, thus exhibiting very similar profiles. Indeed, cholesterol depletion significantly induces activating transcription factor 3 (*ATF3*) at R1h, and high expression levels of *HB-EGF* and *IL-8* are confirmed for all three time points. When analyzed during an 18-hour time-course experiment, the highest *IL-8* gene expression level occurs 2 hours after cholesterol depletion (Supplementary Figure S3 online). *INSIG1*, a gene involved in cellular cholesterol homeostasis, exhibits significantly increased mRNA expression at R1h and R8h after cholesterol depletion (Table 2), indicating cell reaction toward cholesterol synthesis. Expression of matrix metalloproteinase (MMP)1 and MMP10, key regulators of epidermal remodeling during wound healing, is also significantly increased during the delayed recovery phase (R8h; Table 2), with maximal induction of *MMP10* at R4h (Supplementary Figure S3 online). Interestingly, expression profiling of AD patients' keratinocytes has also identified *MMP1* and *MMP10* as major transcriptional targets (Lu *et al.*, 2009). Transcript levels of the urokinase-like plasminogen activator receptor (uPAR or PLAUR) are highly elevated at R1h and R8h (Table 2). Maximal *PLAUR* induction occurs 2 hours after MBCD treatment (Supplementary Figure S3 online). Our data are in accordance with a recent study of vascular smooth muscle cells showing that cholesterol depletion also increases *PLAUR* mRNA levels (Kiyan *et al.*, 2009). Significant increases in *PTGS2* (*COX-2*) expression, a pivotal factor in inflammatory processes, are detected at R1h, R2h, R4h, and R8h after cholesterol extraction (Supplementary Figure S3 online and Table 2).

Analysis of IL-8, PLAU, and PLAUR protein expression

The protein relevance of *IL-8* gene induction after cholesterol depletion by MBCD was investigated by measurement of IL-8 release by keratinocytes (Figure 1a). Compared with control and cholesterol-loaded MBCD-treated cells, cholesterol-depleted keratinocytes secrete significant amounts of IL-8 as early as 2 hours after cholesterol depletion (R2h), reaching maximal levels at late recovery times (R8h and R18h). The urokinase receptor system was more completely explored as PLAUR is localized in lipid rafts (Sitrin *et al.*, 2004) and as PLAU (the expression of which is also augmented in case of

Table 1. List of differentially regulated genes at recovery times 0, 1, and 8 h after cholesterol depletion by methyl-β-cyclodextrin as identified by microarray approach

Upregulated				Downregulated			
Gene symbol	Gene name	Fold change	*P*-value	Gene symbol	Gene name	Fold change	*P*-value
R0h							
FOS	v-fos FBJ murine osteosarcoma viral oncogene homolog	50.3	2.1E−05	*ASPRV1*	Aspartic peptidase, retroviral-like 1	−4.5	2.2E−02
SOCS3	Suppressor of cytokine signaling 3	17.1	1.3E−05	*PTGER4*	Prostaglandin E receptor 4 (subtype EP4)	−3.7	1.0E−02
IL8	Interleukin 8	13.4	3.1E−02	*FLG2*	Filaggrin family member 2	−3.1	2.0E−02
DUSP2	Dual specificity phosphatase 2	11.2	4.9E−04	*FAM13B*	Family with sequence similarity 13, member B	−3.0	2.1E−02
ZFP36	Zinc-finger protein 36, C3H type, homolog (mouse)	9.4	1.1E−02	*EIF5*	Eukaryotic translation initiation factor 5	−2.9	2.4E−15
PTGS2	Prostaglandin-endoperoxide synthase 2 (prostaglandin G/H synthase and cyclooxygenase)	8.2	2.9E−03	*ZNF296*	Zinc-finger protein 296	−2.7	3.3E−02
HBEGF	Heparin-binding EGF-like growth factor	7.8	7.5E−10	*CYP1A1*	Cytochrome P450, family 1, subfamily A, polypeptide 1	−2.5	1.6E−02
IER3	Immediate early response 3	6.0	6.0E−08	*RPL37A*	Ribosomal protein L37a	−2.5	4.2E−02
SLC2A3	Solute carrier family 2 (facilitated glucose transporter), member 3	5.1	4.1E−02	*EIF5*	Eukaryotic translation initiation factor 5	−2.5	2.3E−08
DUSP1	Dual specificity phosphatase 1	4.6	8.3E−07	*ID4*	Inhibitor of DNA binding 4, dominant-negative helix–loop–helix protein	−2.4	1.6E−02
PTGS2	Prostaglandin-endoperoxide synthase 2 (prostaglandin G/H synthase and cyclooxygenase)	4.5	2.0E−07	*CALML5*	Calmodulin-like 5	−2.4	2.4E−04
SPRY2	Sprouty homolog 2 (*Drosophila*)	4.1	5.2E−03	*CNFN*	Cornifelin	−2.3	7.0E−05
DUSP6	Dual specificity phosphatase 6	4.1	1.1E−05	*KIAA1370*	KIAA1370	−2.3	1.8E−03
CXCL2	Chemokine (C–X–C motif) ligand 2	4.1	2.4E−02	*CTGF*	Connective tissue growth factor	−2.2	9.8E−03
PRDM1	PR domain containing 1, with ZNF domain	4.1	1.2E−05	*CST6*	Cystatin E/M	−2.2	5.9E−04
EGR1	Early growth response 1	3.8	1.5E−10	*CALML3*	Calmodulin-like 3	−2.1	9.5E−03
DUSP6	Dual specificity phosphatase 6	3.7	1.2E−05	*FLG*	Filaggrin	−2.1	1.3E−02
PRDM1	PR domain containing 1, with ZNF domain	3.4	2.5E−02	*IFRD1*	Interferon-related developmental regulator 1	−2.1	6.7E−10
SLC2A3	Solute carrier family 2 (facilitated glucose transporter), member 3	3.4	7.8E−03				
TFPI2	Tissue factor pathway inhibitor 2	3.2	6.5E−03				
R1h							
IL-8	Interleukin 8	545.6	4.5E−06	*ZNF434*	Zinc-finger protein 434	−11.4	2.9E−03
IL-8	Interleukin 8	449.9	3.7E−06	*SH3BP5L*	SH3-binding domain protein 5-like	−5.4	3.0E−02
ATF3	Activating transcription factor 3	231.8	1.0E−04	*CYP1A1*	Cytochrome P450, family 1, subfamily A, polypeptide 1	−5.3	1.9E−03
CXCL2	Chemokine (C–X–C motif) ligand 2	174.1	3.0E−05	*PHACTR3*	Phosphatase and actin regulator 3	−5.1	2.8E−02
NR4A1	Nuclear receptor subfamily 4, group A, member 1	127.2	7.7E−03	*NBPF1*	Neuroblastoma breakpoint family, member 1	−4.3	1.0E−02
EGR2	Early growth response 2	124.2	6.4E−03	*C7orf68 (HIG2)*	Chromosome 7 open reading frame 68 (hypoxia inducible gene 2)	−4.2	6.5E−04
IL-20	Interleukin 20	117.2	1.3E−03	*ZNF57*	Zinc-finger protein 57	−3.9	2.1E−04
SLC2A3	Solute carrier family 2 (facilitated glucose transporter), member 3	105.9	1.1E−04	*ZNF14*	Zinc-finger protein 14	−3.9	1.1E−02
DUSP2	Dual specificity phosphatase 2	78.9	4.5E−07	*ZNF557*	Zinc-finger protein 557	−3.9	2.9E−02
PLAUR	Plasminogen activator, urokinase receptor	78.1	1.2E−06	*ZNF12*	Zinc-finger protein 12	−3.8	2.9E−02
PLAUR	Plasminogen activator, urokinase receptor	76.4	1.5E−05	*MGC16385*	Hypothetical protein MGC16385	−3.7	3.9E−03
FOS	v-fos FBJ murine osteosarcoma viral oncogene homolog	71.3	5.4E−06	*ZNF12*	Zinc-finger protein 12	−3.6	2.4E−06
SOCS3	Suppressor of cytokine signaling 3	62.6	2.2E−06	*ASPRV*	Aspartic peptidase, retroviral-like 1	−3.6	3.7E−03
APOBEC3A	Apolipoprotein B mRNA editing enzyme, catalytic polypeptide-like 3A	54.5	7.1E−04	*ATPIF1*	ATPase inhibitory factor 1	−3.5	9.6E−03
NR4A2	Nuclear receptor subfamily 4, group A, member 2	52.9	6.9E−12	*C13orf15*	Chromosome 13 open reading frame 15	−3.5	3.0E−04

Table 1 contained on the following page

Table 1. Continued

Upregulated				Downregulated			
Gene symbol	Gene name	Fold change	*P*-value	Gene symbol	Gene name	Fold change	*P*-value
PTGS2	Prostaglandin-endoperoxide synthase 2 (prostaglandin G/H synthase and cyclooxygenase)	51.8	2.4E−06	*ZNF112*	Zinc-finger protein 112 homolog (mouse)	−3.4	3.2E−03
GEM	GTP-binding protein overexpressed in skeletal muscle	44.5	1.7E−04	*C7orf68 (HIG2)*	Chromosome 7 open reading frame 68 (hypoxia inducible gene 2)	−3.4	1.4E−04
HBEGF	Heparin-binding EGF-like growth factor	44.4	5.6E−14	*ALG12*	Asparagine-linked glycosylation 12, α-1,6-mannosyltransferase homolog (*Saccharomyces cerevisiae*)	−3.3	1.9E−02
SLC2A3	Solute carrier family 2 (facilitated glucose transporter), member 3	42.8	4.0E−10	*FAM13B*	Family with sequence similarity 13, member B	−3.3	9.3E−04
ATF3	Activating transcription factor 3	38.0	1.7E−03	*LOC643008*	Hypothetical protein LOC643008	−3.2	6.2E−03
R8h							
IL1RL1	Interleukin 1 receptor-like 1	2688.5	4.5E−08	*IFIT1*	Interferon-induced protein with tetratricopeptide repeats 1	−159.8	6.5E−04
MMP10	Matrix metallopeptidase 10 (stromelysin 2)	740.7	2.5E−06	*SLC40A1*	Solute carrier family 40 (iron-regulated transporter), member 1	−154.4	2.0E−07
IL13RA2	Interleukin 13 receptor, α-2	306.0	2.4E−07	*EEF2K*	Eukaryotic elongation factor-2 kinase	−97.7	1.2E−04
IL1R2	Interleukin 1 receptor, type II	289.7	1.5E−05	*RAB7B*	RAB7B, member RAS oncogene family	−95.8	1.7E−09
LBH	Limb bud and heart development homolog (mouse)	270.8	1.4E−06	*TNS3*	Tensin 3	−90.7	5.2E−07
SPRY2	Sprouty homolog 2 (*Drosophila*)	265.5	5.3E−06	*ZBTB16*	Zinc-finger and BTB domain containing 16	−81.8	1.5E−04
PTGS2	Prostaglandin-endoperoxide synthase 2 (prostaglandin G/H synthase and cyclooxygenase)	230.0	8.5E−09	*SP100*	SP100 nuclear antigen	−65.2	2.8E−04
TFPI2	Tissue factor pathway inhibitor 2	221.0	2.9E−10	*FOXN3*	Forkhead box N3	−63.6	8.4E−06
ZBED2	Zinc-finger, BED-type containing 2	199.7	8.6E−08	*SKP2*	S-phase kinase-associated protein 2 (p45)	−61.7	4.6E−06
IL-1R2	Interleukin 1 receptor, type II	192.9	1.1E−05	*GHR*	Growth hormone receptor	−59.8	1.7E−06
DEFB103A	Defensin-β 103A	155.6	1.6E−02	*ANLN*	Anillin, actin-binding protein	−55.1	3.1E−07
BMP6	Bone morphogenetic protein 6	141.1	6.9E−06	*BTN3A2*	Butyrophilin, subfamily 3, member A2	−54.6	5.0E−05
CEACAM1	Carcinoembryonic antigen-related cell adhesion molecule 1 (biliary glycoprotein)	133.0	6.3E−08	*ID3*	Inhibitor of DNA binding 3, dominant-negative helix-loop-helix protein	−53.1	3.6E−05
AKAP12	A kinase (PRKA) anchor protein 12	121.5	3.5E−06	*METTL7A*	Methyltransferase like 7A	−46.0	3.0E−08
MUM1L1	Melanoma associated antigen (mutated) 1-like 1	117.6	1.2E−05	*SULT1E1*	Sulfotransferase family 1E, estrogen-preferring, member 1	−44.1	1.7E−04
INHBA	Inhibin β-A	114.7	6.7E−05	*DEPDC7*	DEP domain containing 7	−44.1	5.3E−06
IL-1B	Interleukin 1-β	109.6	1.8E−09	*SULT1E1*	Sulfotransferase family 1E, estrogen-preferring, member 1	−42.4	4.9E−04
MMP1	Matrix metallopeptidase 1 (interstitial collagenase)	103.2	4.6E−08	*MYCL1*	v-Myc myelocytomatosis viral oncogene homolog 1, lung carcinoma derived (avian)	−36.9	2.1E−05
IL-8	Interleukin 8	100.1	1.5E−03	*KRT2*	Keratin 2	−35.8	8.0E−04
AGPAT9	1-Acylglycerol-3-phosphate O-acyltransferase 9	100.0	1.0E−06	*SMAD5OS*	SMAD family member 5 opposite strand	−35.8	1.1E−06

Abbreviations: ATP, adenosine-5′-triphosphate; EGF, epidermal growth factor; GTP, green florescent protein; R0h, cholesterol depletion at 0 hours; R1h, at 1 hour; R8h, at 8 hours.
Shown are the 20 most highly up- and downregulated genes classified according to their fold change (for all genes: adjusted *P*-values <0.05).

cholesterol extraction; Supplementary Figure S2 online) binding to its receptor stimulates cholesterol synthesis (Fuhrman *et al.*, 2007). Highly significant extracellular PLAU release actually occurs between R4h and R8h after the initial cholesterol depletion (Figure 1b). This time schedule exactly corresponds to the recovery period during which the PLAUR protein expression is induced in keratinocytes (Figure 1c), suggesting potential ligand-induced PLAUR activation during this period.

Network and pathway exploration of DRG after membrane cholesterol depletion

To identify potential regulatory networks and pathways from microarray data, lists of DRG after MBCD treatment were uploaded into the bioinformatics tool Ingenuity Pathways Analysis (IPA). IPA's capacity of discriminating relevant functions, pathways, and networks was checked with random gene lists. In reality, IPA analysis reveals that ''cholesterol biosynthesis'' and ''hormone receptor-regulated cholesterol

Table 2. Gene expression levels in methyl-β-cyclodextrin-treated cells compared with untreated keratinocytes[1]

				Microarray					
				Probe set number		*Probe set number*		*Probe set number*	
Gene symbol	**Gene name**	**Recovery time**	**Real-time PCR Fold change[2]**	**Fold change**	***P*-value**	**Fold change**	***P*-value**	**Fold change**	***P*-value**
				HG-U133_Plus_2HF29032		*HG-U133_Plus_2HF13723*		*HG-U133_Plus_2HF20755*	
ATF3	Activating transcription factor 3	0 h	1.15 ± 0.24	15.58	2.2E−01	2.05	2.1E−01	2.24	2.0E−04
		1 h	18.19 ± 6.56	231.84	1.0E−04	37.98	1.7E−03	20.67	1.5E−09
		8 h	1.57 ± 0.42	1.00	2.7E−01	3.96	7.5E−03	1.75	2.3E−02
				HG-U133_Plus_2HF20822					
HBEGF	Heparin-binding EGF-like growth factor	0 h	3.12 ± 0.69	7.79	7.5E−10				
		1 h	27.27 ± 11.19	44.45	5.6E−14				
		8 h	21.57 ± 4.00	33.67	3.9E−13				
				HG-U133_Plus_2HF13928		*HG-U133_Plus_2HF19869*			
IL-8	Interleukin 8	0 h	5.08 ± 1.94	13.39	3.1E−02	2.43	3.3E−02		
		1 h	104.47 ± 43.82	545.62	4.5E−06	449.87	3.7E−06		
		8 h	43.89 ± 10.46	100.11	1.5E−03	37.60	9.9E−05		
				HG-U133_Plus_2HF10596		*HG-U133_Plus_2HF2065*			
INSIG1	Insulin-induced gene 1	0 h	1.03 ± 0.05	1.57	8.9E−04	1.39	5.9E−01		
		1 h	3.68 ± 0.88	7.65	4.2E−12	4.36	2.9E−02		
		8 h	6.15 ± 1.41	10.58	2.1E−10	26.46	2.2E−02		
				HG-U133_Plus_2HF11142					
MMP1	Matrix metalloproteinase 1	0 h	1.44 ± 0.24	2.71	1.4E−02				
		1 h	3.98 ± 1.17	5.80	1.5E−06				
		8 h	114.26 ± 46.68	103.24	4.6E−08				
				HG-U133_Plus_2HF6142					
MMP10	Matrix metalloproteinase 10	0 h	1.28 ± 0.07	1.23	3.4E−01				
		1 h	2.84 ± 0.90	4.94	1.6E−02				
		8 h	307.47 ± 92.43	740.68	2.5E−06				
				HG-U133_Plus_2HF18124		*HG-U133_Plus_2HF21107*		*HG-U133_Plus_2HF3386*	
PLAUR	Plasminogen activator receptor, urokinase type (uPAR)	0 h	1.12 ± 0.05	1.02	6.5E−01	2.36	7.1E−03	2.88	3.5E−02
		1 h	31.13 ± 8.83	10.24	6.6E−04	76.40	1.5E−05	78.06	1.2E−06
		8 h	15.48 ± 2.28	18.06	2.6E−04	32.27	9.5E−07	27.52	3.6E−04
				HG-U133_Plus_2HF19274		*HG-U133_Plus_2HF7077*			
PTGS2	Prostaglandin-endoperoxide synthase 2 (COX-2)	0 h	2.08 ± 0.39	8.16	2.9E−03	4.48	2.0E−07		
		1 h	7.87 ± 2.06	51.81	2.4E−06	11.52	6.1E−08		
		8 h	26.50 ± 10.65	229.97	8.5E−09	75.86	1.7E−06		

Abbreviations: COX-2, cyclooxygenase 2; EGF, epidermal growth factor; FC, fold change; uPAR; urokinase-like plasminogen activator receptor.
[1]Differentially regulated genes are highlighted in gray (quantitative reverse transcriptase PCR: Student's *t*-test with $P<0.05$; microarray: $-2<FC<2$ and adjusted *P*-value <0.05).
[2]Mean fold changes ± SEM from three independent experiments.

metabolism'' are major cellular processes associated with DRG 8 hours after cholesterol depletion (Figure 2a). The gene ontology term ''cholesterol biosynthesis'' contains a set of 16 involved genes, of which 10 are DRGs in the R8h data set (Figure 2b). Among these are key enzymes of cholesterol synthesis, 3-hydroxy-3-methyl-glutaryl-coenzyme A reductase, 3-hydroxy-3-methyl-glutaryl-coenzyme A synthase 1, 7-dehydrocholesterol reductase, and squalene epoxidase, which are all highly upregulated in these conditions. Thus, keratinocytes respond to cholesterol depletion by inducing

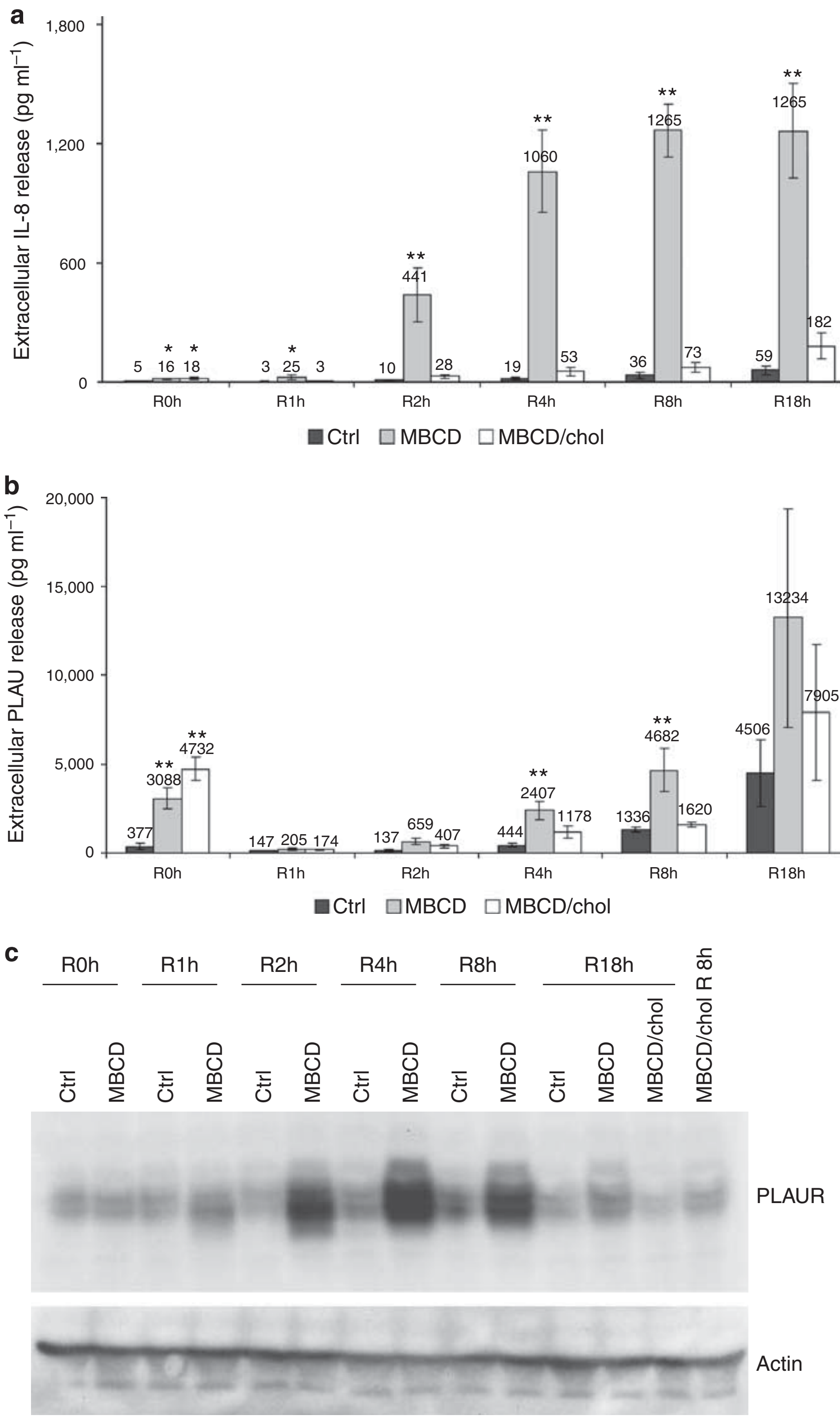

Figure 1. PLAUR expression, and PLAU and IL-8 release after cholesterol depletion. Functional time-course analysis shows that MBCD induces PLAUR protein expression, as well as PLAU and IL-8 protein release. (**a**) Extracellular IL-8 release subsequent to MBCD and MBCD/chol treatments (means ± SEM; $n=4$). (**b**) Extracellular PLAU release subsequent to MBCD and MBCD/chol treatments (means ± SEM; $n=3$). (**c**) Western blot analysis of PLAUR protein expression in cell lysates of cholesterol-depleted keratinocytes (representative data obtained from three independent experiments). chol, cholesterol; Crtl, control, MBCD, methyl-β-cyclodextrin; PLAU, plasminogen activator urokinase; PLAUR, plasminogen activator urokinase receptor; R0h, cholesterol depletion at 0 hours; R1h, at 1 hour; R2h, at 2 hours; R4h, at 4 hours, R18h, at 18 hours. *$P<0.05$; **$P<0.01$; Dunnett's test.

the transcription of genes encoding cholesterol synthesis enzymes as early as 8 hours after MBCD treatment.

Functional IPA annotation (Supplementary Figure S4 online) illustrates that two categories of diseases, namely, ''reproductive system disease'' and ''dermatological diseases and conditions'', are major gene ontology terms associated with DRG at R0h, R1h, and R8h. These bioinformatics results might be explained by the fact that steroid hormones are

a

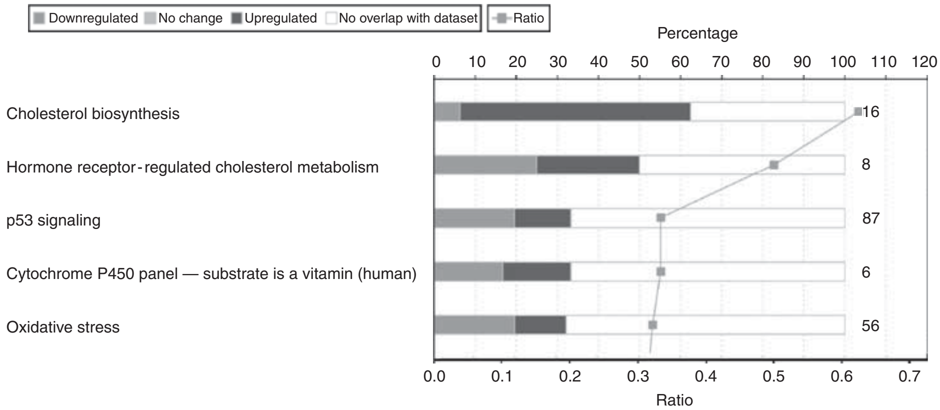

b

Symbol	Entrez gene name	Fold change	*P*-value	Location	Type
ACAT1	Acetyl-coenzyme A acetyltransferase 1	−2.336	2.19E-04	Cytoplasm	Enzyme
ACAT2	Acetyl-coenzyme A acetyltransferase 2	3.345	4.59E-03	Cytoplasm	Enzyme
DHCR7	7-Dehydrocholesterol reductase	2.829	1.15E-06	Cytoplasm	Enzyme
EBP	Emopamil binding protein (sterol isomerase)	2.337	2.08E-04	Cytoplasm	Enzyme
FDFT1	Farnesyl-diphosphate farnesyltransferase 1	—	—	—	—
FDPS	Farnesyl diphosphate synthase	3.488	1.30E-02	Cytoplasm	Enzyme
HMGCR	3-Hydroxy-3-methylglutaryl-coenzyme A reductase	2.969	1.40E-04	Cytoplasm	Enzyme
HMGCS1	3-Hydroxy-3-methylglutaryl-coenzyme A synthase 1 (soluble)	10.201	3.56E-06	Cytoplasm	Enzyme
HMGCS2	3-Hydroxy-3-methylglutaryl-coenzyme A synthase 2 (mitochondrial)	—	—	—	—
IDI1	Isopentenyl-diphosphate delta isomerase 1	4.566	7.23E-09	Cytoplasm	Enzyme
LSS	Lanosterol synthase	—	—	—	—
MVD	Mevalonate (diphospho) decarboxylase	9.361	1.67E-05	Cytoplasm	Enzyme
MVK	Mevalonate kinase	—	—	—	—
PMVK	Phosphomevalonate kinase	—	—	—	—
SC5DL	Sterol-C5-desaturase (ERG3 delta-5-desaturase homolog, s. cerevisiae)-like	—	—	—	—
SQLE	Squalene epoxidase	5.104	1.25E-06	Cytoplasm	Enzyme

Figure 2. Differentially regulated genes. Illustration of the most highly represented functional groups from the list of differentially regulated genes R8h (cholesterol depletion at 8 hours) (**a**) and details on genes involved in the cholesterol biosynthesis pathway (**b**). (**a**) Ingenuity Pathway Analysis (IPA)-generated major functions of differentially regulated genes at R8h. Light gray: downregulated gene expression; dark gray: upregulated gene expression. In all, 10 of the 16 genes present in the group ''cholesterol biosynthesis'' are regulated (corresponding to 62.5%), one gene is downregulated (6.25%), and nine genes are upregulated (56.25%). (**b**) IPA list of the 16 genes involved in ''cholesterol biosynthesis'' and their fold changes and *P*-values when differentially regulated in the methyl-β-cyclodextrin R8h dataset.

produced from cholesterol and that cholesterol depletion perturbs endocrine steroid regulatory mechanisms.

Potential networks for cholesterol-depleted keratinocytes generate previously unreported working hypotheses and identify critical mediators of AD pathways

At R0h after cholesterol depletion, a potential network involving *TGFB1*, *IL-6*, and *IL-8* is suggested by IPA analysis. The presence of *PTGS2*, *activating transcription factor 3*, and *PLAUR* in this network is remarkable (Figure 3a).

Thereafter, a second network centered on tumor necrosis factor-α is top-scored at time point R1h (Figure 3b), featuring *HB-EGF*, *IL-8*, *PTGS2*, and *MMP1* as possibly tumor necrosis factor-α-regulated genes in cholesterol-depleted keratinocytes. Interestingly, ''dermatological diseases and conditions'' and ''inflammatory disease'' are key terms associated with this network.

Finally, at time point R8h, the inflammatory network prevails, featuring ILs-1α and -β as central factors. In this network, MMP1, 3, and 9, as well as PTGS2 and IL-8, have very important roles (Figure 3c).

Functional annotation analysis of DRGs revealed that ''dermatological diseases and conditions'' was a function strongly associated with R0h and R1h data sets, a highly interesting result as standard IPA settings were used. Therefore, we investigated which dermatological disease associates best. AD associates the most significantly with the transcriptional profile observed at R0h, and AD is second at R1h after lipid raft disruption by MBCD (Supplementary Figure S5 online). Intersection of MBCD-regulated genes and genes related to AD include *IL-8*, *PTGS2*, *IL-1RN*, *SOCS3*, *DUSP1*, *DUSP2*, *DUSP5*, and transcription factors *JUN*, *JUNB*, and *ZFP36* (all of which are upregulated) and the only downregulated epidermal gene *FLG* (Supplementary Figure S5 online).

Having identified a potential relationship between cholesterol depletion and AD, links between dermatitis and the top-scored networks were found, and highlighted in blue in Figure 3. Each of the networks illustrates at least five genes involved in the disease, suggesting that cholesterol depletion could mimic certain features of AD.

Transcript levels of cholesterol-regulated genes that are members of the epidermal differentiation cluster are shown in Figure 4a. To test whether cholesterol depletion has crucial effects on genes that are deregulated in AD, skin biopsy specimens of acute lesions and surrounding normal-appearing skin of AD patients (average age: 39 years), as well as biopsy specimens of healthy volunteers (average age: 43 years), were collected after informed consent. When performing comparisons between groups of AD patients and healthy persons, no age-related effects were observed. Using real-time PCR, transcript levels of several major targets of cholesterol depletion were analyzed (Figure 4b–h). The mean expression of late differentiation markers *FLG* and loricrin (*LOR*) is approximately twofold significantly decreased in AD skin (either lesional or non-lesional) when compared with healthy skin (Figure 4b and c). Inside or outside AD lesions, no difference in the expression of these two genes could be detected. *IVL* and transglutaminase (*TGM-1)* exhibit similar mRNA levels in both healthy and non-lesional AD skin, whereas expression of these two genes is increased for every patient, leading to a significant mean increase in *IVL* and *TGM-1* in lesional compared with non-lesional AD skin (Figure 4d and e). In healthy patients, the expression level of *HB-EGF* presents a high variability, especially in two samples, probably as a consequence of the collecting procedure, *HB-EGF* being an early stress-responsive gene (Mathay *et al*., 2008). In samples from AD patients, the non-lesional *HB-EGF* expression level is low but increases significantly in lesional areas of most AD patients (Figure 4f). Similarly, *IL-8* transcript levels exhibit particularly high values in lesional AD skin, compared with either non-lesional areas or healthy samples (Figure 4g), revealing the important inflammatory response in acute AD lesions. Regarding *PLAUR* expression levels, no tendency in expression can be detected between healthy and non-lesional AD skin; however, each AD patient reveals an increase in *PLAUR* transcript levels in lesions compared with levels in non-lesional areas (Figure 4h) and the average *PLAUR* expression is significantly increased in lesional AD skin. Thus, elevated *IL-8*, *PLAUR*, *HB-EGF*, and *TGM1* expression can be considered as a previously unreported gene signature of inflammatory lesional AD plaques.

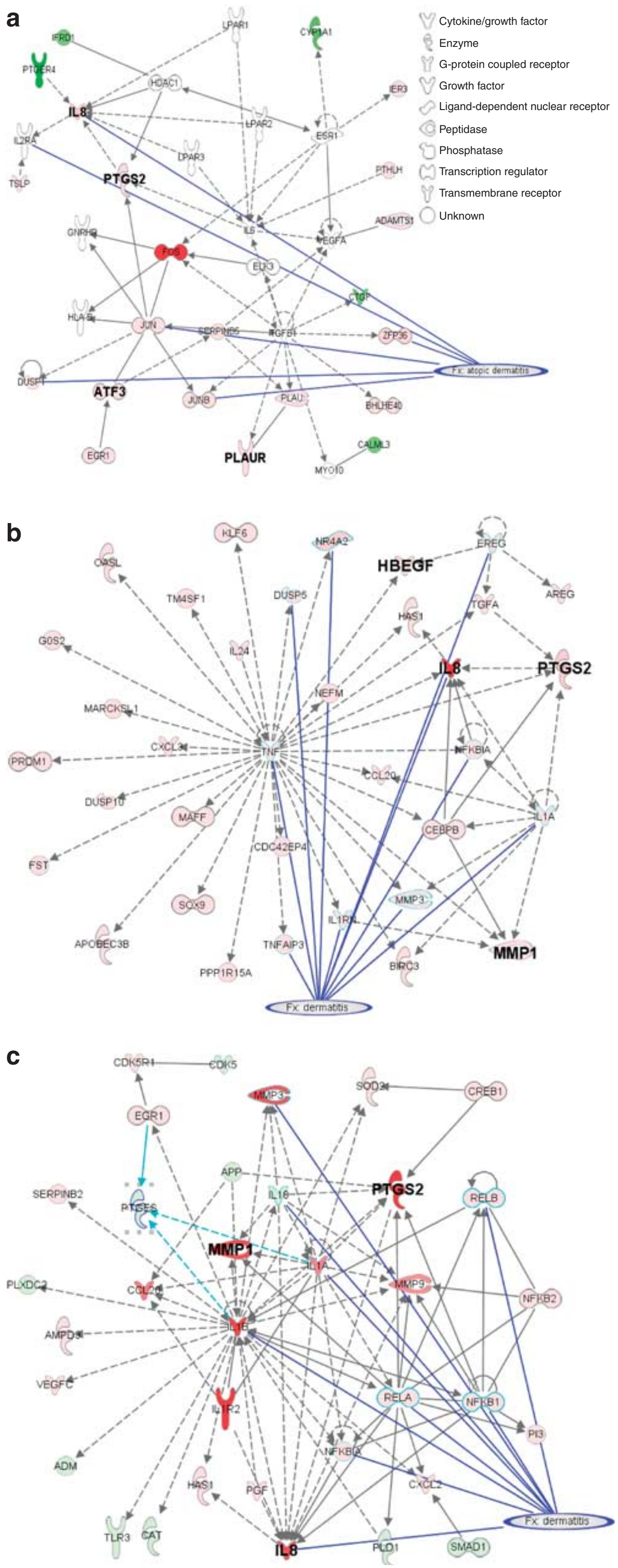

Figure 3. Potential networks and interactions. Illustration of potential networks showing relevant genes and their possible interactions, either immediately after cholesterol depletion (at 0 hours (R0h (**a**)) or after recovery times of 1 hour (R1h (**b**)) or 8 hours (R8h (**c**)). Full arrows indicate direct interactions, whereas dotted arrows indicate indirect interactions. Upregulated genes are indicated in red color, whereas green color indicates downregulated genes. Intense colors indicate high fold changes. Genes known to be involved in dermatitis are indicated by blue lines. The shape of the node indicates the major function of the protein. Data were analyzed by the Ingenuity Pathway Analysis 7.5 tool. ATF3, activating transcription factor; HB-EGF, heparin-binding EGF-like growth factor; MMP1, metalloproteinase 1; PLAUR, plasminogen activator urokinase receptor; PTGS2, prostaglandin-endoperoxide synthase 2.

In summary, when comparing AD skin with normal skin, increased expression levels of *IVL*, *TGM1*, *HB-EGF*, *IL-8*, and *PLAUR* are detected simultaneously with a decreased expression of *FLG* and *LOR*. These observations are in good concordance with transcriptional analysis of gene expression in lipid raft-disrupted keratinocytes, strongly suggesting that membrane organization and signaling might be disturbed in AD keratinocytes.

DISCUSSION

Genome expression profiling in cholesterol-depleted keratinocytes reveals hundreds of DRGs as an immediate or later consequence of lipid raft disruption. Such a strong transcriptional regulation may likely be explained by the fact that lipid rafts are known to host large numbers of signaling molecules that cannot form competent signaling assemblies after cholesterol extraction. Data presented here illustrate that processes initiated by cholesterol depletion are complex and dynamic, involving IL-8, HB-EGF, and PLAUR, for instance, among major transcriptional targets, an observation confirmed by protein analysis and showing the physiological importance of cholesterol-dependent gene expression in keratinocytes.

IL-8 and PLAU induction and secretion, together with HB-EGF release (Giltaire and Poumay, unpublished results), as a consequence of lipid raft disruption are to our best knowledge previously unreported results. IL-8 is an inflammatory marker induced by various stress signals and recently EGFR-dependent IL-8 synthesis has been shown in wounded keratinocytes, a process that contributes to injury-initiated neutrophil recruitment (Roupé *et al.*, 2010).

Highly elevated PLAUR transcript levels are also detected after cholesterol depletion (Figure 1). The urokinase system PLAU/PLAUR is mainly known for its fibrinolytic function during tissue remodeling; however, PLAUR is also involved in cell adhesion, migration, and signaling (Ragno, 2006; Caceres *et al.*, 2008). Further investigations of this urokinase system represent promising areas of research because cholesterol biosynthesis is increased not only by PLAU binding to its receptor (Fuhrman *et al.*, 2007) but also because PLAU secretion and increased PLAUR expression are induced as a response to cholesterol depletion. Thus, the PLAU/PLAUR system may be suspected to enhance cholesterol biosynthesis. Moreover, PLAU binding to its receptor increases the lipid raft affinity of this GPI-anchored receptor (Sahores *et al.*, 2008). In prostate cells, PLAU is able to stimulate autocrine HB-EGF production, thereby maintaining EGFR activation (Caceres *et al.*, 2008). A similar mechanism might function in keratinocytes after cholesterol depletion as PLAU secretion is observed (Figure 1b) and HB-EGF is simultaneously released (Giltaire and Poumay, in preparation). Furthermore, it has been shown that, in keratinocytes, EGFR activation depends on PLAUR membrane expression (D'Alessio *et al.*, 2008). EGFR is activated immediately after cholesterol depletion (Jans *et al.*, 2004; Lambert *et al.*, 2008), probably because the required basal PLAUR levels are present, but PLAUR levels are also highly increased during the recovery period after cholesterol depletion. Finally, our data concur with a study conducted on vascular smooth muscle cells showing PLAUR induction following cholesterol depletion (Kiyan *et al.*, 2009).

In our present data, gene ontology analysis of DRG after cholesterol depletion in keratinocytes has pointed out AD as the dermatological disease that best fits the gene regulation obtained by cholesterol depletion. Thus, we tested whether major genes regulated after lipid rafts disruption by cholesterol depletion could similarly be regulated in AD skin biopsies. Indeed, data revealed good concordance between AD and lipid raft disruption.

Since the discovery of an increased risk of AD in patients carrying *FLG* mutations (Palmer *et al.*, 2006), the involvement of epidermal differentiation cluster genes in etiopathology of AD has drawn considerable scientific interest. In AD skin, a decreased expression of *FLG* is generally observed (Sugiura *et al.*, 2005; Guttman-Yassky *et al.*, 2009) and might contribute to the impaired epidermal barrier of acute AD lesions. Our data also illustrate significantly decreased *FLG* and *LOR* expression in AD, together with increased *IVL*, perfectly matching literature data (Sugiura *et al.*, 2005; Howell *et al.*, 2007; Jarzab *et al.*, 2010), as well as data observed in cholesterol-depleted keratinocytes. Thus, three members of the epidermal differentiation cluster are similarly regulated in AD and in keratinocytes with disrupted lipid rafts. In addition, an interesting increase in SOCS3 expression and PLAUR activity is detected in AD (Saaf *et al.*, 2008; Voegeli *et al.*, 2009), similar to that in cholesterol-depleted keratinocytes. Finally, although individual gene expression variations occur, no particular age-related effect could be identified between cohorts of patients.

Intriguing parallelisms in our data strongly suggest that keratinocyte lipid rafts could be involved in the etiopathology of AD, maybe by impaired lipid raft organization or perturbed signaling in AD. Interestingly, during the process of epidermal barrier maturation, lamellar bodies exhibit properties of lipid rafts (Menon, 2003); indeed lamellar bodies are enriched in caveolin-1, a lipid raft marker protein (Sando *et al.*, 2003), and the fusion of lamellar bodies with the apical plasma membrane of granular keratinocytes is regulated by membrane cholesterol (Roelandt *et al.*, 2009). Thus, as a correct exocytosis of lamellar bodies is required for the function of the epidermal barrier, and as lamellar body formation and delivery mechanisms are perturbed in AD, leading to an impaired epidermal barrier (Fartasch *et al.*, 1992), the functioning of keratinocyte lipid rafts could be compromised in AD. Moreover, a profiling study in AD patients has recently revealed a marked differential regulation of genes involved in lipid biosynthesis (Saaf *et al.*, 2008), genes that are also regulated after lipid raft disruption (Figure 2). These data provide additional support for the hypothetical involvement of lipid rafts in AD. Finally, data from recent literature demonstrate that miltefosine, an alkylphospholipid with high affinity for lipid rafts (Barratt *et al.*, 2009) and presented as a potential lipid raft modulator, can significantly attenuate allergic sensitization (Weller *et al.*, 2009). Miltefosine has also been successfully tested in mice and human AD treatment

a

	MBCD vs ctrl		
Gene symbol	FC	*P*-value	Recovery time
FLG	−2.11	0.01251	R0h
FLG2	−3.10	0.02034	R0h
FLG2	−16.91	0.00011	R8h
LOR	−4.28	0.00319	R8h
IVL	2.40	0.00003	R8h
TGM1	4.55	0.00486	R8h

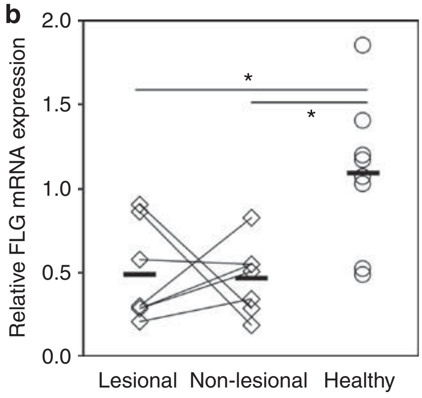

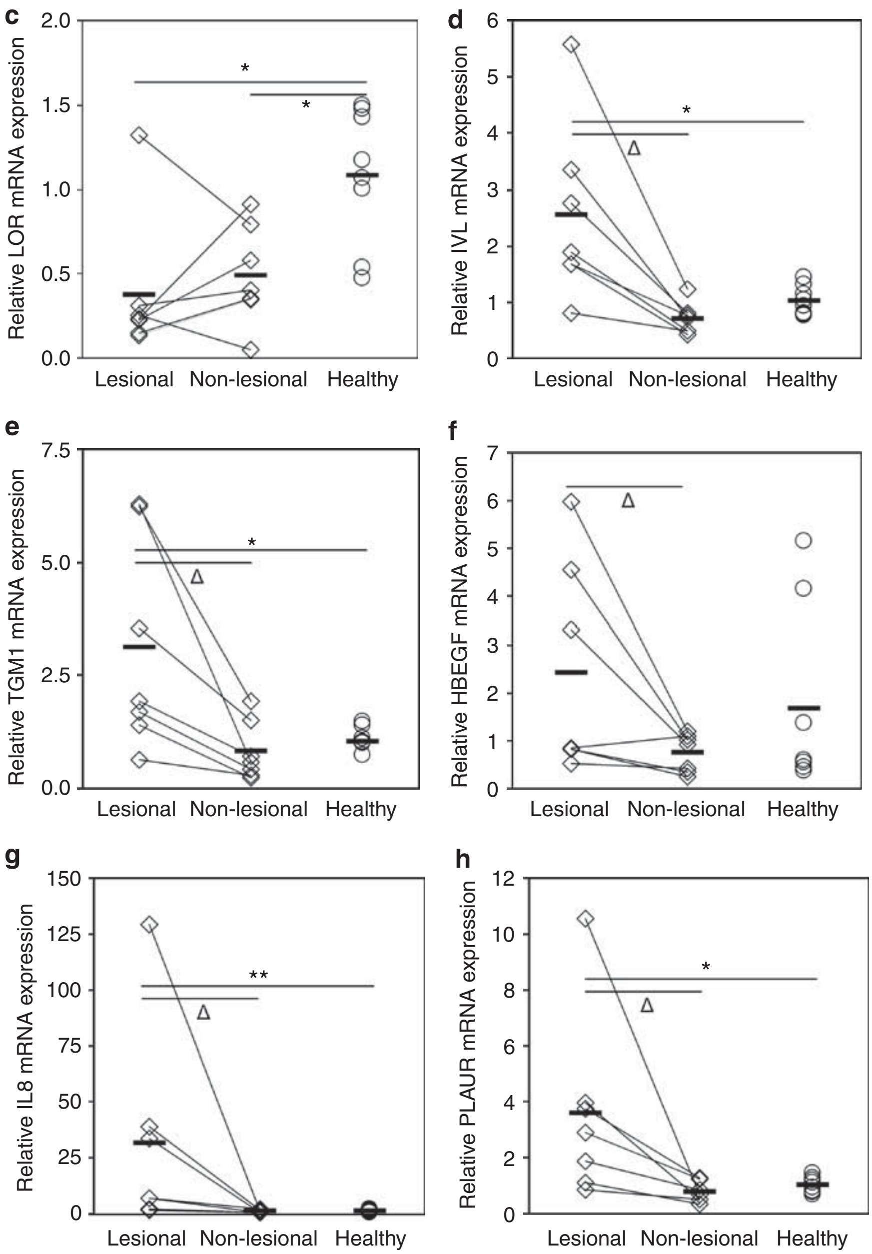

(Bäumer *et al.*, 2010; Dölle *et al.*, 2010), bringing an additional argument for our hypothesis.

Altogether, this study first contributes to a better knowledge of epidermal lipid rafts and their associated signaling, as it demonstrates their physiological relevance in keratinocytes in inducing IL-8, PLAU, and PLAUR, in addition to HB-EGF. Second, the detailed analysis of signaling pathways perturbed by lipid raft disruption has identified crucial mediators involved in the etiopathology of AD.

MATERIALS AND METHODS

Chemicals and culture media

MBCD and cholesterol were obtained from Sigma-Aldrich (Bornem, Belgium). Keratinocyte growth medium 2 was purchased from Clonetics (Lonza, Verviers, Belgium). Keratinocyte complete culture medium (Epilife with human keratinocyte growth supplement) and keratinocyte autocrine culture medium (Epilife without human keratinocyte growth supplement) were from Cascade Biologics (Invitrogen, Merelbeke, Belgium).

Skin biopsies and culture of human normal epidermal keratinocytes

This study was conducted in accordance with the Declaration of Helsinki. The study was approved by the Ethics Committee of the University Hospital Center of Liège and by the medical ethical committee of Clinique St Luc, Namur. The whole procedure of the study was fully explained to all volunteers who gave their written informed consent. None of the AD patients were receiving any topical or systemic therapy other than hydrating creams. Supplementary Table S2 online summarizes demographic data of seven AD volunteers suffering from longstanding AD who underwent a skin biopsy on lesional and surrounding non-lesional skin and of eight healthy volunteers. Superficial 2 mm punch biopsies, composed of mainly epidermis with minimal dermis amounts, were taken from AD patients under local anesthesia and then stored in RNAlater (Qiagen, Venlo, The Netherlands) before RNA extraction (RNeasy Micro, Qiagen) and real-time PCR analysis. For healthy samples and *in vitro* culture experiments, abdominal or breast skin samples obtained from plastic surgery were used and keratinocyte cultures were grown in autocrine culture medium until confluence as described earlier(Minner *et al.*, 2010).

Lipid raft disruption by cholesterol depletion

Cholesterol depletion in confluent keratinocyte cultures was performed by 7.5 mM (1% wt/vol) MBCD for 1 hour. For mock cholesterol depletion (negative control), cells were incubated for 1 hour with 7.5 mM cholesterol-loaded MBCD complexes (cholesterol-loaded MBCD; Klein *et al.*, 1995). Cells were harvested either immediately after MBCD treatment (R0h) or were allowed to recover in autocrine culture medium for 1 hour (R1h) or 8 hours (R8h).

Microarray and bioinformatics analyses

Detailed microarray and bioinformatics analyses are described in Supplementary Methods online. Briefly, tRNA integrity was analyzed (Agilent 2100 Bioanalyzer; Agilent, Santa Rosa, CA) and whole-genome expression levels were determined on Affymetrix HG-U133 Plus 2.0 GeneChips (Affymetrix, Sunnyvale, CA). Probe sets with a fold change >2 or <-2 and a *P*-value lower than 0.05 were defined to be differentially regulated and were selected for further analyses. In compliance with minimum information about a microarray experiment standards, data files were deposited into the NCBI Gene Expression Omnibus. The Gene Expression Omnibus accession number is GSE21364. http://www.ncbi.nlm.nih.gov/geo/query/acc.cgi?acc=GSE21364.

Network generation and functional analysis of microarray data

Lists of DRGs with associated fold changes and *P*-values were imported into the Ingenuity Pathway Analysis 7.5 tool (Ingenuity Systems, Redwood City, CA). The basis of the IPA tool consists of the Ingenuity Pathway Knowledge Base, which is derived from known functions and published gene interactions. The most relevant biological networks, functions, or pathways of a data set were identified by a Fischer's exact test computing a *P*-value that determines the probability that the network, function, or pathway assigned to that data set is because of chance alone.

Real-time PCR protocol and primer sequences (Supplementary Table S1 online) are available in online Supplementary Methods online.

Protein extraction and western blotting

Immediately after the indicated treatments, cells were washed with phosphate-buffered saline and harvested in twice-concentrated Laemmli sample buffer without dithiothreitol (62.5 mM Tris–HCl, 2% SDS, 8.7% glycerol, 0.05% bromophenol blue). Proteins were analyzed by SDS-PAGE and by blotting onto polyvinylidene fluoride membranes (GE Healthcare Bio-Sciences, Uppsala, Sweden). Blocking of the membrane was followed by incubation with primary antibodies against PLAUR (R&D Systems, Abigdon, UK) and β-actin (Sigma-Aldrich, Bornem, Belgium), followed by incubation with secondary antibodies. Chemoluminescent detection was carried out as described previously (Mathay *et al.*, 2008).

IL-8/PLAU measurement

IL-8 and PLAU protein concentrations were measured in cell culture medium using commercial quantitative sandwich immunoassays (Duoset, R&D systems, Abigdon, UK). Each sample was assayed in duplicate according to the manufacturer's instructions, and detection was carried out at 450 nm (wavelength correction: 540 nm) in a microplate reader (VersaMax Molecular Devices, Sunnyvale, CA). IL-8 and PLAU concentrations were calculated following standard curves.

Figure 4. Gene expression in keratinocytes and skin samples. Relative mRNA expression levels of genes of the epidermal differentiation cluster are analyzed in cholesterol-depleted keratinocytes (**a**) and gene transcript levels are analyzed in lesional and non-lesional skin of seven atopic dermatitis (AD) patients and in skin of eight healthy volunteers (**b–h**). Demographic data are available in Supplementary Table S2. Expression levels of filaggrin (FLG, **b**), loricrin (LOR, **c**), involucrin (IVL, **d**), transglutaminase-1 (TGM1, **e**), HB-EGF (heparin-binding EGF (epidermal growth factor)-like growth factor, **f**), IL-8 (**g**), and PLAUR (plasminogen activator urokinase receptor, **h**) were normalized to the average expression of two housekeeping genes (*RPLP0* and *TBP*). Values are expressed relatively to the means of eight healthy volunteers. Statistical analyses were performed by a paired Wilcoxon signed-rank test for the comparison of lesional versus non-lesional AD skin (Δ: $P<0.05$) and by a Mann–Whitney test (Bonferroni corrected) for the comparisons of lesional versus healthy skin and of non-lesional versus healthy skin (*$P<0.05$, **$P<0.01$). –, mean value; ctrl, control; FC, fold change; FLG2, filaggrin-2.

CONFLICT OF INTEREST

The authors state no conflict of interest.

ACKNOWLEDGMENTS

We thank Karen A Squillace for her availability and her excellent technical help with microarray experiments. CM is a research fellow and AC is a senior research associate of the ''Fonds de la Recherche Scientifique-FNRS''. MP is a research fellow of the FRIA. This work was financially supported by FNRS grant 1.5.033.06F and FRFC grant 2.4.522.10F to YP.

SUPPLEMENTARY MATERIAL

Supplementary material is linked to the online version of the paper at http://www.nature.com/jid

REFERENCES

Barratt G, Saint-Pierre-Chazalet M, Loiseau PM (2009) Cellular transport and lipid interactions of miltefosine. *Curr Drug Metab* 10:247–55

Bäumer W, Wlaz P, Jennings G *et al.* (2010) The putative lipid raft modulator miltefosine displays immunomodulatory action in T-cell dependent dermal inflammation models. *Eur J Pharmacol* 628:226–32

Brint EK, Xu D, Liu H *et al.* (2004) ST2 is an inhibitor of interleukin 1 receptor and Toll-like receptor 4 signaling and maintains endotoxin tolerance. *Nat Immunol* 5:373–9

Caceres M, Tobar N, Guerrero J *et al.* (2008) c-jun-NH2JNK mediates invasive potential and EGFR activation by regulating the expression of HB-EGF in a urokinase-stimulated pathway. *J Cell Biochem* 103:986–93

D'Alessio S, Gerasi L, Blasi F (2008) uPAR-deficient mouse keratinocytes fail to produce EGFR-dependent laminin-5, affecting migration *in vivo* and *in vitro*. *J Cell Sci* 121:3922–32

Dölle S, Hoser D, Rasche C *et al.* (2010) Long-term reduction in local inflammation by a lipid raft molecule in atopic dermatitis. *Allergy* 65:1158–65

Fartasch M, Bassukas ID, Diepgen TL (1992) Disturbed extruding mechanism of lamellar bodies in dry non-eczematous skin of atopics. *Br J Dermatol* 127:221–7

Foster LJ (2008) Lessons learned from lipid raft proteomics. *Expert Rev Proteomics* 5:541–3

Fuhrman B, Nitzan O, Karry R *et al.* (2007) Urokinase plasminogen activator (uPA) stimulates cholesterol biosynthesis in macrophages through activation of SREBP-1 in a PI3-kinase and MEK-dependent manner. *Atherosclerosis* 195:e108–16

Gniadecki R, Bang B (2003) Flotillas of lipid rafts in transit amplifying cell-like keratinocytes. *J Invest Dermatol* 121:522–8

Guttman-Yassky E, Suarez-Farinas M, Chiricozzi A *et al.* (2009) Broad defects in epidermal cornification in atopic dermatitis identified through genomic analysis. *J Allergy Clin Immunol* 124:1235–44 e1258

Howell MD, Kim BE, Gao P *et al.* (2007) Cytokine modulation of atopic dermatitis filaggrin skin expression. *J Allergy Clin Immunol* 120:150–5

Jans R, Atanasova G, Jadot M *et al.* (2004) Cholesterol depletion upregulates involucrin expression in epidermal keratinocytes through activation of p38. *J Invest Dermatol* 123:564–73

Jarzab J, Filipowska B, Zebracka J *et al.* (2010) Locus 1q21 Gene expression changes in atopic dermatitis skin lesions: deregulation of small proline-rich region 1A. *Int Arch Allergy Immunol* 151:28–37

Kabouridis PS, Janzen J, Magee AL *et al.* (2000) Cholesterol depletion disrupts lipid rafts and modulates the activity of multiple signaling pathways in T lymphocytes. *Eur J Immunol* 30:954–63

Kiyan J, Smith G, Haller H *et al.* (2009) Urokinase-receptor-mediated phenotypic changes in vascular smooth muscle cells require the involvement of membrane rafts. *Biochem J* 423:343–51

Klein U, Gimpl G, Fahrenholz F (1995) Alteration of the myometrial plasma membrane cholesterol content with beta-cyclodextrin modulates the binding affinity of the oxytocin receptor. *Biochemistry* 34:13784–93

Lambert S, Ameels H, Gniadecki R *et al.* (2008) Internalization of EGF receptor following lipid rafts disruption in keratinocytes is delayed and dependent on p38 MAPK activation. *J Cell Physiol* 217:834–45

Lambert S, Vind-Kezunovic D, Karvinen S *et al.* (2006) Ligand-independent activation of the EGFR by lipid raft disruption. *J Invest Dermatol* 126:954–62

Lange Y, Ye J, Steck TL (2004) How cholesterol homeostasis is regulated by plasma membrane cholesterol in excess of phospholipids. *Proc Natl Acad Sci USA* 101:11664–7

Lu ZR, Park D, Lee KA *et al.* (2009) Profiling the dysregulated genes of keratinocytes in atopic dermatitis patients: cDNA microarray and interactomic analyses. *J Dermatol Sci* 54:126–9

Mathay C, Giltaire S, Minner F *et al.* (2008) Heparin-binding EGF-like growth factor is induced by disruption of lipid rafts and oxidative stress in keratinocytes and participates in the epidermal response to cutaneous wounds. *J Invest Dermatol* 128:717–27

Mathay C, Poumay Y (2010) Lipid rafts and the oxidative stress hypothesis. *J Invest Dermatol* 130:1457–9

Menon GK (2003) Caveolins in epidermal lamellar bodies: skin is an interactive interface, not an inflexible barrier. *J Invest Dermatol* 120:xv–i

Minner F, Herphelin F, Poumay Y (2010) Study of epidermal differentiation in human keratinocytes cultured in autocrine conditions. *Methods Mol Biol* 585:71–82

Oyoshi MK, He R, Kumar L *et al.* (2009) Cellular and molecular mechanisms in atopic dermatitis. *Adv Immunol* 102:135–226

Palmer CN, Irvine AD, Terron-Kwiatkowski A *et al.* (2006) Common loss-of-function variants of the epidermal barrier protein filaggrin are a major predisposing factor for atopic dermatitis. *Nat Genet* 38: 441–6

Pike LJ (2006) Rafts defined: a report on the keystone symposium on lipid rafts and cell function. *J Lipid Res* 47:1597–8

Pike LJ (2009) The challenge of lipid rafts. *J Lipid Res* 50(Suppl):S323–8

Ragno P (2006) The urokinase receptor: a ligand or a receptor? Story of a sociable molecule. *Cell Mol Life Sci* 63:1028–37

Roelandt T, Giddelo C, Heughebaert C *et al.* (2009) The ''caveolae brake hypothesis'' and the epidermal barrier. *J Invest Dermatol* 129:927–36

Roupé KM, Nybo M, Sjobring U *et al.* (2010) Injury is a major inducer of epidermal innate immune responses during wound healing. *J Invest Dermatol* 130:1167–77

Saaf AM, Tengvall-Linder M, Chang HY *et al.* (2008) Global expression profiling in atopic eczema reveals reciprocal expression of inflammatory and lipid genes. *PLoS One* 3:e4017

Sahores M, Prinetti A, Chiabrando G *et al.* (2008) uPA binding increases UPAR localization to lipid rafts and modifies the receptor microdomain composition. *Biochem Biophys Acta* 1778:250–9

Sando GN, Zhu H, Weis JM *et al.* (2003) Caveolin expression and localization in human keratinocytes suggest a role in lamellar granule biogenesis. *J Invest Dermatol* 120:531–41

Shi L, Jones WD, Jensen RV *et al.* (2008) The balance of reproducibility, sensitivity, and specificity of lists of differentially expressed genes in microarray studies. *BMC Bioinformatics* 9(Suppl 9):S10

Simons K, Toomre D (2000) Lipid rafts and signal transduction. *Nat Rev Mol Cell Biol* 1:31–9

Sitrin RG, Johnson DR, Pan PM *et al.* (2004) Lipid raft compartmentalization of urokinase receptor signaling in human neutrophils. *Am J Respir Cell Mol Biol* 30:233–41

Sugiura H, Ebise H, Tazawa T *et al.* (2005) Large-scale DNA microarray analysis of atopic skin lesions shows overexpression of an epidermal differentiation gene cluster in the alternative pathway and lack of protective gene expression in the cornified envelope. *Br J Dermatol* 152:146–9

Voegeli R, Rawlings AV, Breternitz M *et al.* (2009) Increased stratum corneum serine protease activity in acute eczematous atopic skin. *Br J Dermatol* 161:70–7

Weller K, Artuc M, Jennings G *et al.* (2009) Miltefosine inhibits human mast cell activation and mediator release both *in vitro* and *in vivo*. *J Invest Dermatol* 129:496–8

Wertz PW, Michniak BB (2000) Epidermal lipid metabolism and barrier function of stratum corneum. In: *Biochemical Modulation of Skin Reactions* (Kydonieus AF, Wille JJ, eds). CRC Press, 35–44

Wu Z, Hansmann B, Meyer-Hoffert U *et al.* (2009) Molecular identification and expression analysis of filaggrin-2, a member of the S100 fused-type protein family. *PLoS One* 4:e5227

Yaqoob P, Shaikh SR (2010) The nutritional and clinical significance of lipid rafts. *Curr Opin Clin Nutr Metab Care* 13: 156–66

Supplementary Data and Methods

Figure S1: Confirmation of known cholesterol-depletion induced effects on cell signalling molecules and mRNA expression of selected genes

a

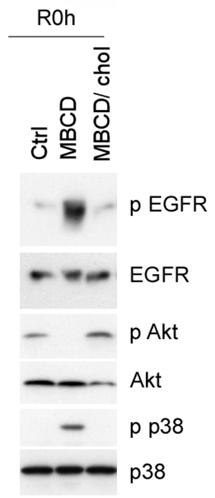

b

		Microarray HG-U133_Plus_2				Real-time PCR		
		MBCD vs Ctrl		MBCD/chol vs Ctrl		Ctrl	MBCD	MBCD/chol
Official gene symbol	Recovery time	FC	p value	FC	p value	FC ± SEM	FC ± SEM	FC ± SEM
HBEGF	0h	7,79	7,5E-10	1,80	3,8E-05	1,00 ± 0,11	2,99 ± 0,23	1,04 ± 0,09
	1h	44,45	5,6E-14	8,02	5,3E-11	1,00 ± 0,20	22,00 ± 9,70	3,95 ± 1,26
	8h	33,67	3,9E-13	2,30	6,5E-05	1,00 ± 0,19	20,87 ± 10,48	1,47 ± 0,30
KRT10	0h	*-1,17*	2,0E-02	*-1,17*	1,3E-02	1,00 ± 0,27	*-1,56 ± 0,59*	*-1,54 ± 0,37*
	1h	*-1,16*	1,4E-02	*-1,30*	2,2E-08	1,00 ± 0,30	1,44 ± 0,63	*-1,22 ± 0,37*
	8h	*-1,72*	1,3E-02	*-1,39*	1,7E-01	1,00 ± 0,30	*-4,32 ± 1,28*	*-2,18 ± 0,88*
IVL	0h	*-1,34*	2,6E-05	*-1,41*	2,4E-04	1,00 ± 0,33	*-1,55 ± 0,29*	*-1,50 ± 0,30*
	1h	*-1,01*	8,9E-01	*-1,38*	2,6E-05	1,00 ± 0,24	1,11 ± 0,24	*-1,30 ± 0,22*
	8h	2,40	2,6E-05	*-1,03*	9,4E-01	1,00 ± 0,32	4,09 ± 2,03	1,06 ± 0,27
TGM1	0h	*-1,05*	5,4E-01	*-1,36*	3,8E-01	1,00 ± 0,26	*-1,47 ± 0,31*	*-1,47 ± 0,31*
	1h	*-1,19*	4,2E-03	*-1,50*	2,5E-02	1,00 ± 0,18	*-1,24 ± 0,09*	*-1,43 ± 0,32*
	8h	4,55	4,9E-03	*-1,04*	7,9E-01	1,00 ± 0,56	4,83 ± 4,81	*-1,08 ± 0,49*

Figure S1: Confirmation of known cholesterol-depletion induced effects on cell signalling molecules and mRNA expression of selected genes. a. Western blot analysis of proteins extracted immediately after treatment (R0h) from untreated confluent keratinocytes cultures, cholesterol-depleted keratinocytes (7.5 mM MBCD for 1h) or mock cholesterol-depleted keratinocytes (7.5 mM MBCD/chol for 1h). b. mRNA expression analysis of HB-EGF, the early differentiation marker keratin 10 (KRT10) and the late differentiation markers involucrin and transglutaminase-1 (TGM1) in untreated keratinocytes (Ctrl), in 7.5mM MBCD-treated keratinocytes and in 7.5mM MBCD/chol-treated keratinocytes, immediately after the treatment (R0h) or after 1h or 8h recovery (R1h respectively R8h), by microarray technique and real-time PCR (3 independent experiments). Differential gene regulations are indicated in gray.

Microarray analysis

The integrity of tRNA samples was analysed (Agilent 2100 Bioanalyser) and whole genome expression measurements were performed on Affymetrix HG-U133 Plus 2.0 GeneChips®. Nine arrays were used for the three conditions (Ctrl, MBCD and MBCD/chol) tested at each of the three time points (R0h, R1h and R8h). Microarray analysis was conducted according to manufacturer's instructions for the Affymetrix One Cycle Target Labeling and Control Reagents kit (Santa Clara, CA). Briefly, cDNA was generated from 1.5 µg of total RNA using SuperScript II reverse transcriptase (Invitrogen, Carlsbad, CA) and T7 Oligo(dT) primer. Subsequently, the products were column-purified (Affymetrix) and then in vitro transcribed to generate biotin-labeled cRNA. The IVT products were then column-purified, fragmented, and hybridized onto Affymetrix U133 Plus 2.0 GeneChips® at 45º C for 16 h. Subsequent to hybridization, the arrays were washed and stained with

streptavidin-phycoerythrin, then scanned in an Affymetrix GeneChip® Scanner 3000 (Santa Clara, CA). All control parameters were confirmed to be within normal ranges before normalization and data reduction was initiated. CEL files were obtained and an alternative CDF from AffyProbeMiner (Liu *et al.*, 2007) was used to link digitalized signals to gene names. AffyProbeMiner assigns the 1.400.000 probes of HG-U133 Plus 2.0 to 23.800 probe sets representing the whole human genome. The CDF used is « transcript-consistent », so each probe of a probe set maps to the same set of transcripts. The minimal size of a probe set was set to five probes (Liu *et al.*, 2007). Gene annotation by AffyProbeMiner resulted for some genes in the fact that multiple probe sets correspond to one gene. Pre-processing was performed with GCRMA (Wu *et al.*, 2004) with default parameters. For each probe set, fold changes (ratio of expression between two conditions) (Draghici, 2002) were calculated for six comparisons (for each time point MBCD versus Ctrl and MBCD/chol versus Ctrl). ANOVA 2 with conditions and probes as levels (Barrera *et al.*, 2004) was performed to measure the statistical significance of differential expression for each probe set in the six comparisons. P values were adjusted for multiple testing using False Discovery Rate analysis (Benjamini and Hochberg, 1995). Probe sets with a fold change higher than 2 or lower than -2 and a p-value lower than 0.05 were defined to be differentially regulated and were selected for further analyses. The entire analysis was made with the R statistical software (Ihaka and Gentleman, 1996) and packages from Bioconductor (Gentleman *et al.*, 2004). In compliance with MIAME standards, data files were deposited into the NCBI Gene Expression Omnibus (GEO). The following link was created to allow review of these data: The GEO accession number is GSE21364.
http://www.ncbi.nlm.nih.gov/geo/query/acc.cgi?acc=GSE21364

Real-time PCR

RNA extraction (RNeasy, Qiagen, Hilden, Germany), reverse transcription (Super Script II RNase H (Invitrogen, Merelbeke, Belgium) and real-time PCR were done as described by Mathay *et al.* (2008) with primer sequences listed in Table S1. Each reaction (40 cycles comprising each 15 seconds at 95°C and 1 min at 60°C) was performed using Power SYBR Green PCR Master Mix (Applied Biosystems) in a 7300 real-time PCR machine (Applied Biosystems, Lennik, Belgium). The specificity of the PCR products was verified by melting curves. TBP and RPLP0 had previously been selected for gene expression normalization by GeNorm analysis and relative gene expression was calculated as described by Minner and Poumay (2009). Fold changes were calculated for the six comparisons: MBCD versus Ctrl and MBCD/chol versus Ctrl for each of the three time points.

Table S1: real-time PCR primers

Gene Symbol	Forward primer (5' - 3')	Reverse primer (5' - 3')
ATF3	ACCTCTGCCACCGGATGTC	GTCGCCTCTTTTTCCTTTCATCT
HBEGF	TGGCCCTCCACTCCTCATC	GGGTCACAGAACCATCCTAGCT
FLG	GGGCACTGAAAGGCAAAAAG	CACCATAATCATAATCTGCACTACCA
IL8	GCAGAGGGTTGTGGAGAAGTTT	TTGGATACCACAGAGAATGAATTTTT
INSIG1	CTCTTCCCCGAGGAGGTGAT	TCCGAGGTGACTGTCGATACAG
IVL	TGAAACAGCCAACTCCAC	TTCCTCTTGCTTTGATGGG
LOR	TCATGATGCTACCCGAGGTTTG	CAGAACTAGATGCAGCCGGAGA
MMP1	AGCTAGCTCAGGATGACATTGATG	GCCGATGGGCTGGACAG
MMP10	TTCCAGGAGTTGAGCCTAAGGT	AAACTGTGATGATCCACTGAAGAAGT
PLAUR	GACCTCTGCAGGACCACGAT	CGATAGCTCAGGGTCCTGTTG
PTGS2	CCTTCCTCCTGTGCCTGATG	ACAATCTCATTTGAATCAGGAAGCT
RPLP0	ATCAACGGGTACAAACGAGTC	CAGATGGATCAGCCAAGAAGG
TBP	TCAAACCCAGAATTGTTCTCCTTAT	CCTGAATCCCTTTAGAATAGGGTAGA
TGM1	GTCGTCTTCCGGCTCGAA	TCACTGTTTCATTGCCTCCAAT

Figure S2 is an Excel file (GSE21364_fold_change_data.xls.gz) which is available online on GEO: http://www.ncbi.nlm.nih.gov/geo/query/acc.cgi?acc=GSE21364

Figure S2: Differentially up- and down-regulated genes in MBCD- respectively MBCD/chol treated confluent keratinocyte cultures analysed immediately after treatment (R0h) or after 1h respectively 8h of recovery (R1h respectively R8h).

Figure S3: Time-course study of IL8, PTGS2, MMP10 and PLAUR mRNA expression in cholesterol-depleted or mock cholesterol-depleted keratinocytes.

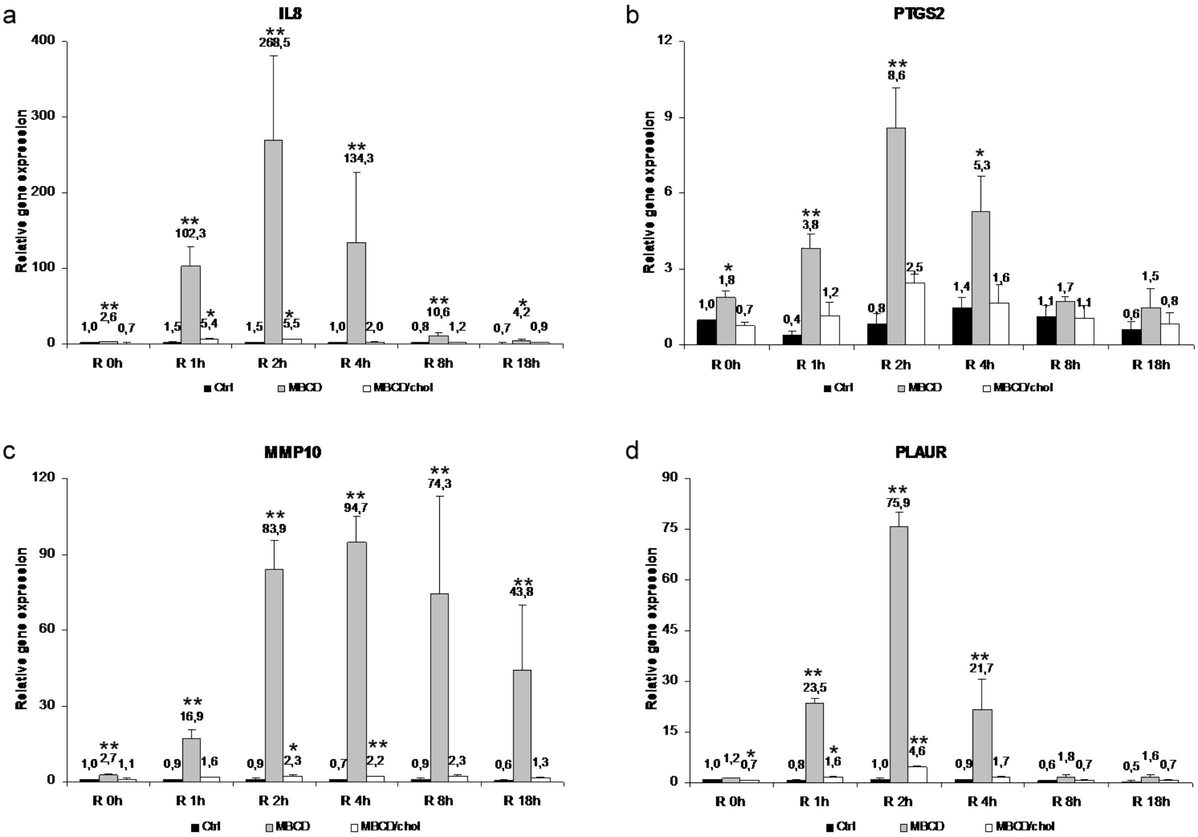

Figure S3: Time-course study of IL8 (**A**), PTGS2 (**B**), MMP10 (**C**) and PLAUR (**D**) mRNA expression in cholesterol-depleted or mock cholesterol-depleted keratinocytes. Real-time PCR data are expressed relative to the control time point R1h. Illustrated data show mean mRNA expression values +/- SEM levels (IL8: n=4; PTGS2, MMP10, PLAUR: n=3 for each). Statistical ANOVA1 analysis was performed after testing the homogeneity of variance (Bartlett). To ensure homoskedasticity, values for IL8, MMP10 and PLAUR were replaced by their logarithmic values. Post hoc comparisons were performed by Dunnett's test. (*: $p<0.05$, **: $p<0.01$).

Figure S4: Representation of the major biological functions assigned to differentially regulated genes

a

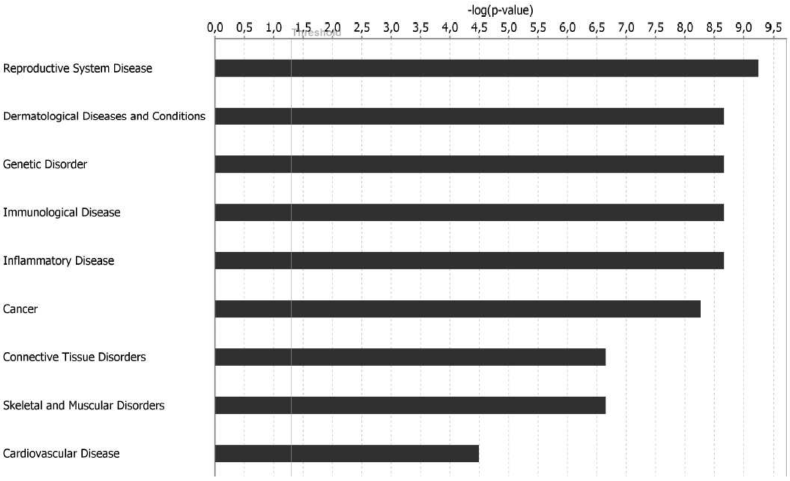

b

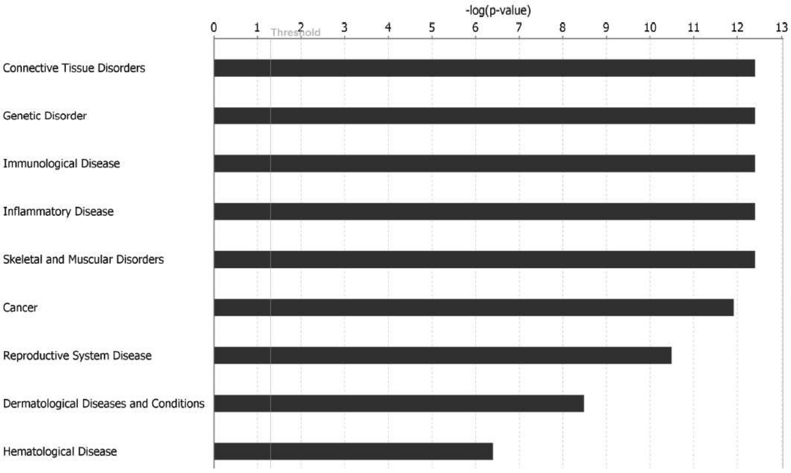

c

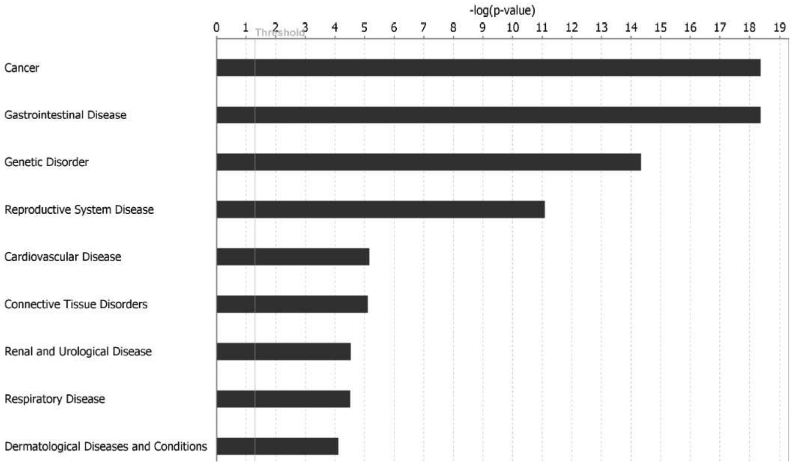

Figure S4: Comparison analysis of the nine most significant biological functions assigned to differentially regulated genes for time points R0h (a), R1h (b) and R8h (c). Biological functions include the three subheadings: diseases and disorders, molecular and cellular functions, physiological system development and function. Significance (-log (p-value)) is indicated by the height of the bars. The x-axis crosses the y-axis at the 1.3 threshold of significance (-log (p=0.05)=1.3) (IPA 7.5).

Figure S5: Relevant functional groups of the category "Dermatological diseases and Conditions" and their transcriptional regulation after cholesterol depletion

Recovery time	Function	Function Annotation	p-value	Genes	Number of Genes
R0h	atopic dermatitis	atopic dermatitis	2,17E-09	DUSP1, DUSP2, ***FLG***, IL8, JUN, JUNB, SOCS3, ZFP36	8
	dermatological disorder	dermatological disorder	5,04E-07	CCL20, DUSP1, DUSP2, ***FLG***, HBEGF, IL8, JUN, JUNB, MMP1, PTGS2, SOCS3, ZFP36	12
	disease	disease of skin	1,54E-04	HBEGF, IL8	2
R1h	dermatitis	Dermatitis	3,26E-09	DUSP1, DUSP2, DUSP5, EIF1, HRH1, IDI1, IL8, IL1RN, JUN, JUNB, MYC, NR4A2, SOCS3, TNFAIP3, ZFP36	15
	atopic dermatitis	atopic dermatitis	3,66E-08	DUSP1, DUSP2, EIF1, HRH1, IDI1, IL8, IL1RN, JUN, JUNB, NR4A2, SOCS3, TNFAIP3, ZFP36	13
	dermatological disorder	dermatological disorder	1,75E-05	AREG, CCL20, ***DLX3***, DUSP1, DUSP2, DUSP5, EIF1, EPHA2, GJB3, HBEGF, HRH1, IDI1, IL8, IL1RN, JUN, JUNB, ***LOR***, MMP1, MYC, NR4A2, PTGS2, SOCS3, TNF, TNFAIP3, ZFP36, ZNF750	26
R8h	apoptosis	apoptosis of epithelial cell lines	7,74E-05	***ALDH3A1, APP***, BIRC3, ***BNIP3***, CD44, CFLAR, ***FAS***, IER3, ***IGFBP3***, ITGA5, ***MAP3K5***, PPARD, PPP1R15A, ***PYCARD***, TGFB1, TIAM1, TICAM1, ***TMX1***, TNFRSF25, TNFRSF10A, ***TNFRSF10B***, ***TNFSF10, TP53***, TP53BP2, TRIB3, XIAP	26
	cell death	cell death of epithelial cell lines	8,02E-05	***ABCG2, ALDH3A1, APP***, BIRC3, ***BNIP3, CAT***, CD44, CFLAR, EMP1, ***FAS***, IER3, IGFBP3, ITGA5, ***MAP3K5***, NAMPT, PPARD, PPP1R15A, ***PYCARD***, ***SIRT3***, TGFB1, TIAM1, TICAM1, ***TMX1***, TNFRSF25, TNFRSF10A, ***TNFRSF10B***, ***TNFSF10, TP53***, TP53BP2, TRIB3, XIAP	31
	actinic keratosis	actinic keratosis	1,69E-03	ALAD, GPX2, PTGS1, PTGS2, TP53, TYMS	6

Figure S5: Illustration of the highest represented functional groups of the category "Dermatological Diseases and Conditions" and description of the transcriptional regulation of the involved genes. Upregulated genes are indicated in normal characters, downregulated genes are in bold and italic characters. Data were analysed by IPA 7.5.

Table S2: Volunteers demographics

Volunteer	Age/sex	Biopsy site	Degree of inflammation	IgE level UI/ml	RAST
1	25 y f	arm	+++	179	D Pter 2/6
2	57 y m	trunc	+++	ND	ND
3	73 y m	trunc	++	14780	D Pter 6/6
4	12 y f	arm	+++++	84	D Pter 4/6
5	39 y m	trunc	+++	146	D Pter 1/6
6	30 y f	arm	++++	23	D Pter 0/6
7	37 y m	arm	+++	829	D Pter 1/6
8	32 y f	breast	0	/	/
9	52 y f	breast	0	/	/
10	21 y f	breast	0	/	/
11	24 y f	lower abdomen	0	/	/
12	64 y f	lower abdomen	0	/	/
13	49 y f	breast	0	/	/
14	60 y f	breast	0	/	/
15	45 y f	lower abdomen	0	/	/

Y: years, f: female, m: male.

References for Supplementary Methods

Barrera L, Benner C, Tao YC, Winzeler E, Zhou Y (2004) Leveraging two-way probe-level block design for identifying differential gene expression with high-density oligonucleotide arrays. *BMC Bioinformatics* 5:42.

Benjamini Y, Hochberg Y (1995) Controlling the False Discovery Rate - a Practical and Powerful Approach to Multiple Testing. *Journal of the Royal Statistical Society Series B-Methodological* 57:289-300.

Draghici S (2002) Statistical intelligence: effective analysis of high-density microarray data. *Drug Discov Today* 7:S55-63.

Gentleman RC, Carey VJ, Bates DM, Bolstad B, Dettling M, Dudoit S, *et al.* (2004) Bioconductor: open software development for computational biology and bioinformatics. *Genome Biol* 5:R80.

Ihaka R, Gentleman R (1996) R : a language for data analysis and graphics. *J Computational and Graphical Stat* 5:16.

Liu H, Zeeberg BR, Qu G, Koru AG, Ferrucci A, Kahn A, *et al.* (2007) AffyProbeMiner: a web resource for computing or retrieving accurately redefined Affymetrix probe sets. *Bioinformatics* 23:2385-2390.

Mathay C, Giltaire S, Minner F, Bera E, Herin M, Poumay Y (2008) Heparin-binding EGF-like growth factor is induced by disruption of lipid rafts and oxidative stress in keratinocytes and participates in the epidermal response to cutaneous wounds. *J Invest Dermatol* 128:717-727.

Minner F, Poumay Y (2009) Candidate housekeeping genes require evaluation before their selection for studies of human epidermal keratinocytes. *J Invest Dermatol* 129:770-773.

Wu ZJ, Irizarry RA, Gentleman R, Martinez-Murillo F, Spencer F (2004) A model-based background adjustment for oligonucleotide expression arrays. *Journal of the American Statistical Association* 99:909-917.